Comparison between experiments and Large-Eddy Simulations of tip spiral structure and geometry

Stefan Ivanell, Thomas Leweke, Sasan Sarmast, Hugo Umberto Quaranta, Robert F Mikkelsen, Jens Nørkær Sørensen

Comparison between experiments and Large-Eddy Simulations of tip spiral structure and geometry

2015 J. Phys.: Conf. Ser. 625 012018

(http://iopscience.iop.org/1742-6596/625/1/012018)

Comparison between experiments and Large-Eddy Simulations of tip spiral structure and geometry

S. Ivanell[1,2], T. Leweke[3], S. Sarmast[1], H.U. Quaranta[3], R.F. Mikkelsen[4], J.N. Sørensen[1,4]

[1]Uppsala University, Wind Energy Section, Campus Gotland, 621 67 Visby, Sweden
[2]KTH Mechanics, 100 44 Stockholm, Sweden
[3]IRPHE, CNRS, Aix-Marseille Université, Centrale Marseille, 13384 Marseille, France
[4]Wind Energy Department, Technical University of Denmark, 2800 Lyngby, Denmark

E-mail: stefan.ivanell@geo.uu.se

Abstract.

Results from Large-Eddy Simulations using the actuator line technique have been validated against experimental results. The experimental rotor wake, which forms the basis for the comparison, was studied in a recirculating free-surface water channel, where a helical vortex was generated by a single-bladed rotor mounted on a shaft. An investigation of how the experimental blade geometry and aerofoil characteristics affect the results was performed. Based on this, an adjustment of the pitch setting was introduced, which is still well within the limits of the experimental uncertainty. Excellent agreement between the experimental and the numerical results was achieved concerning the circulation, wake expansion and pitch of the helical tip vortex. A disagreement was found regarding the root vortex position and the axial velocity along the centre line of the tip vortex. This work establishes a good base for further studies of more fundamental stability parameters of helical rotor wakes.

1. Introduction

Studies focusing on understanding the stability properties of the wakes generated by wind turbine rotors have been intensified during the last decade. The reason is that wind farms are becoming larger and larger and therefore the importance of a better understanding of the wake physics is becoming more and more important.

The stability of tip vortex systems has been studied by Widnall [1] and Leishman *et al.* [2], with the main emphasis on helicopter rotors. In 2010, Ivanell *et al.* [3] performed a numerical investigation of the tip spiral instability of a wind turbine wake. This work has been followed up by Sarmast *et al.* [4] and by Sørensen *et al.* [5].

Experimental studies of wind turbine tip spiral instabilities have been carried out by Leweke *et al.* [6] and Bolnot [7]. In general, the stability results by Leweke *et al.* [6] agree well with the results of Ivanell *et al.* [3] and Sarmast *et al.* [4]. However, no study known to the authors have been performed to make a detailed comparison between experiments and simulations considering the same configuration, with focus on tip spiral instability.

With this article we take the first step towards a thorough comparison between an experimental study and a numerical method. When studying instabilities of tip vortices of a wind turbine using experimental methods, the detailed turbine characteristics are usually not

of importance, since the aim in that case is to establish a realistic helical vortex system. It is of course important that the blades are identical and that there is no pitch offset in order not to introduce disturbances to the spiral system. But the design of the blades, the lift and drag force characteristics, are not an essential ingredient, as long as realistic distributions are employed. However, when comparing experimental studies with numerical methods, the detailed knowledge of the blade design is needed. In this study, the rotor is simulated using the actuator line method, in which the detailed geometry of the blades are not needed. Instead, aerofoil characteristics, i.e., lift and drag distributions, together with twist and chord length distributions, are essential. Considering the scale of the turbine, which in this specific case has a radius $R_0 = 80$ mm, the aerofoil characteristics, and especially the drag component, is difficult to establish, because of the low Reynolds number.

Before being able to make a comprehensive numerical/experimental comparison of the breakdown process of the tip spiral system, as it was performed separately by e.g. Sarmast *et al.* [4] and Leweke *et al.* [6], there are many challenges to ensure an adequate comparison of the basic wake configuration. The aim of this article is to establish a comparison of the main flow properties, to conclude on how different parameters match and to quantify the differences due to the setup of the experiment and the numerical method. Studies of the stability of the helical system will therefore not be included in this study, but will be treated in future work.

2. Experiments

The experimental rotor wake, which is the basis for the present comparison, was studied in the recirculating free-surface water channel at IRPHE Marseille, having a test section of dimensions 38 cm (height) × 50 cm (width) × 150 cm (length). A helical vortex was generated near the test section entry by a single-bladed rotor mounted on an ogive-tipped shaft (diameter 15 mm) and driven by a computer-controlled stepper motor outside the channel using a belt (figure 1a). The rotor blade geometry, shown schematically in figure 1(b), is based on the low-Reynolds number airfoil A18 by Selig *et al.* [8]. It is designed to operate in the wind turbine regime and produce a constant radial circulation distribution (Joukowsky rotor) over the outer 75% of the span, in order to generate a highly concentrated tip vortex. The (measured) chord and twist distributions of the blade are shown in figure 3, they correspond to the design distributions. The rotor has a radius $R_0 = 80$ mm and a tip chord $c_{tip} = 10$ mm. Details of the design procedure, as well as the experimental set-up and procedure, can be found in Bolnot [7] and Quaranta *et al.* [9]. For the present experiments, the blade is rotated at a frequency $f_0 = 6$ Hz, and placed in a uniform incoming flow of velocity $U_0 = 36$ cm/s. This results in a tip chord-based Reynolds number of about 30000 and a tip speed ratio $2\pi f_0 R_0/U_0 = 8.4$, representing the design conditions for the blade geometry. No cavitation occurred for these parameter values.

For the comparison, it is of utmost importance that the geometry of the rotor used in the comparison is identical to the one used in the experiments. The experimental set-up was initially not designed for an accurate analysis of rotor blade aerodynamics, but for the study of helical vortex dynamics in the rotor wake, for which a precise blade alignment was not needed. The relatively simple mounting of the rotor object (figure 1) on the shaft resulted in a limited precision of the alignment of the blade with respect to the axis of rotation. Although the mounting was always done in the same way, this could result in a constant offset of the order of 1° in the twist distribution of figure 3(b). Since it was not possible to measure this offset experimentally, the relevant value was found from comparison with numerical simulations. In figure 3 we show, as an example, the experimental evolution of the wake radius and various corresponding numerical results obtained for different twist offsets β. It is found that an offset angle of $\beta = 1.5°$ gives the best agreement between experiment and simulation. Additional comparisons (not shown) were also made for the other wake parameters discussed in section 4, resulting in the same optimal offset. Hence, this value is the one used in the following; the corresponding twist distribution is

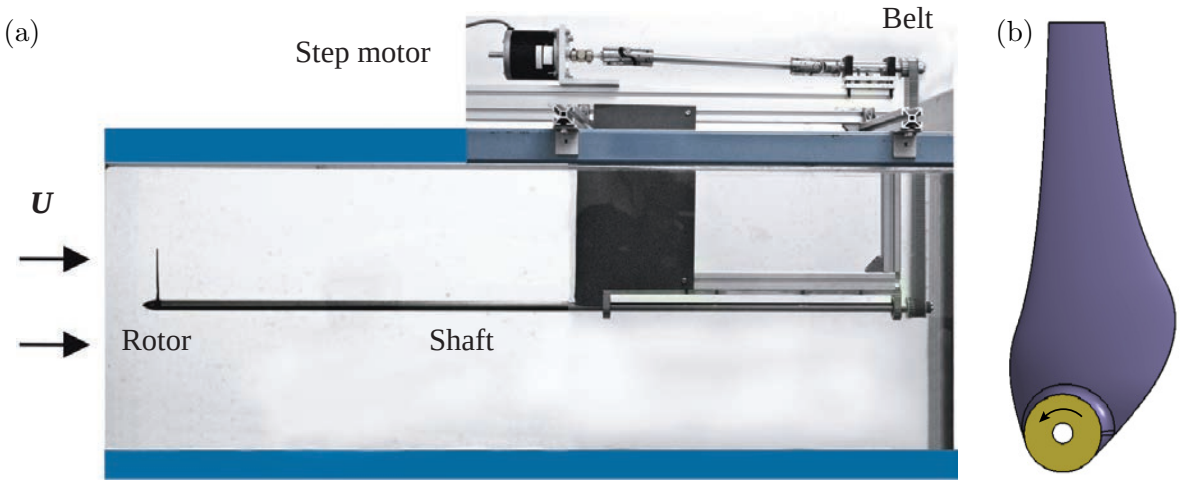

Figure 1. (a) Experimental set-up (side view of the water channel test section) and (b) schematic of the rotor blade geometry.

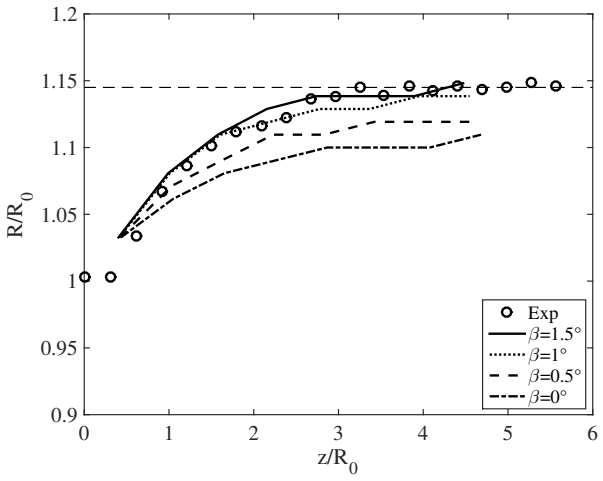

Figure 2. Downstream evolution of helix radius. β is the blade pitch offset.

shown as a line in figure 3.

The vortex structures are visualized using fluorescent dye illuminated by the light of an argon ion laser. The dye is either washed off the blade tip or injected at a fixed location near the blade tip trajectory. Quantitative measurements were carried out using two-component Particle-Image Velocimetry [11] in planes containing the helix axis. Further details can be found in [7] and [9].

3. Numerical method and setup

The actuator line (ACL) method was introduced by Sørensen & Shen [10], as an aerodynamic model for simulating rotor wakes. In this approach, the flow around the rotor is governed by the three-dimensional incompressible Navier–Stokes equations, while the influence of the blades on the flow field is approximated by body forces. These forces, which are determined using the local flow field combined with tabulated airfoil data, and are distributed radially along a line representing the blade of the wind turbine. At each point of the line, the force is smeared among neighboring nodes with a three-dimensional Gaussian smearing function [11]. The ACL method is implemented into the EllipSys3D code, developed by Michelsen [12] and Sørensen

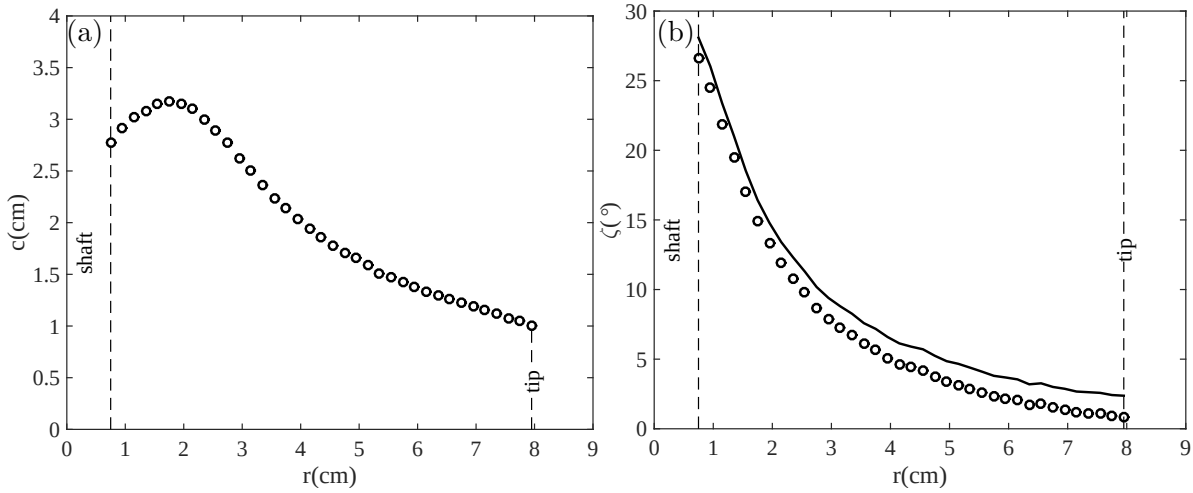

Figure 3. Radial distributions of (a) chord c and (b) twist angle ζ of the blade. Measurements ($\circ$) and twist distribution used in the computations (—).

[13]. Large-Eddy Simulation (LES) is employed, in which the large scales are resolved and the small scales are modeled by the eddy viscosity based sub-grid scale model by Ta Phouc [14]. The computations are conducted using an axisymmetric 360° polar grid with 49 million grid points, in which each blade is represented by an actuator line of 105 grid points. The simulations are performed in a rotating frame of reference, where the actuator lines are standing still. In order to replicate experimental blockage effects, a cross section area corresponding to the one of the water tunnel is considered.

The current simulations are based on the operating conditions of the experiments, where the rotor operates at its design condition. Previous studies of Hansen *et al.* [15] and Sarmast *et al.* [16] show that the accuracy of the actuator line approach is directly related to the quality of the airfoil characteristics. Figure 4 shows the airfoil characteristics used in rotor computations. Prior measured 2D characteristics of an A18 airfoil has been reported for aerodynamic coefficients above $Re_c = 40000$, together with the lift coefficient distributions at $Re_c = 30000$. Xfoil computations are performed to obtain the missing drag coefficients at $Re_c = 30000$.

4. Results

4.1. Helical vortices

Figures 5(a) and 5(b) show the helical vortices produced by the one-bladed rotor operating at its optimum condition $\lambda = 8.4$ for the experiments and the actuator line computations, respectively. In the experiments, fluorescent dye is washed off from the blade tip, while the helical vortices are visualised using an iso-surface of the vorticity magnitude. This visual comparison indicates a very good qualitative agreement between the experiment and the simulation.

Figure 6 illustrates the downstream evolution of the helix radius, i.e. the wake expansion, and the helix pitch. The agreement is again very good.

Figure 7 shows a comparison between experimental and numerical results of the local vorticity in the vortex core. We here consider a helical vortex filament in a cylindrical reference frame (r, θ, z) linked to the rotor geometry, while an additional cylindrical reference frame (ρ, ϕ, ξ), linked locally to the tip vortex, is introduced.

The phase-averaged azimuthal (with respect to the rotor) vorticity field in the near-wake centre plane of the rotor, obtained from 100 instantaneous PIV fields, is shown in figure 7(a). Figure 7(b) shows the azimuthally (with respect to the vortex) averaged velocity profile

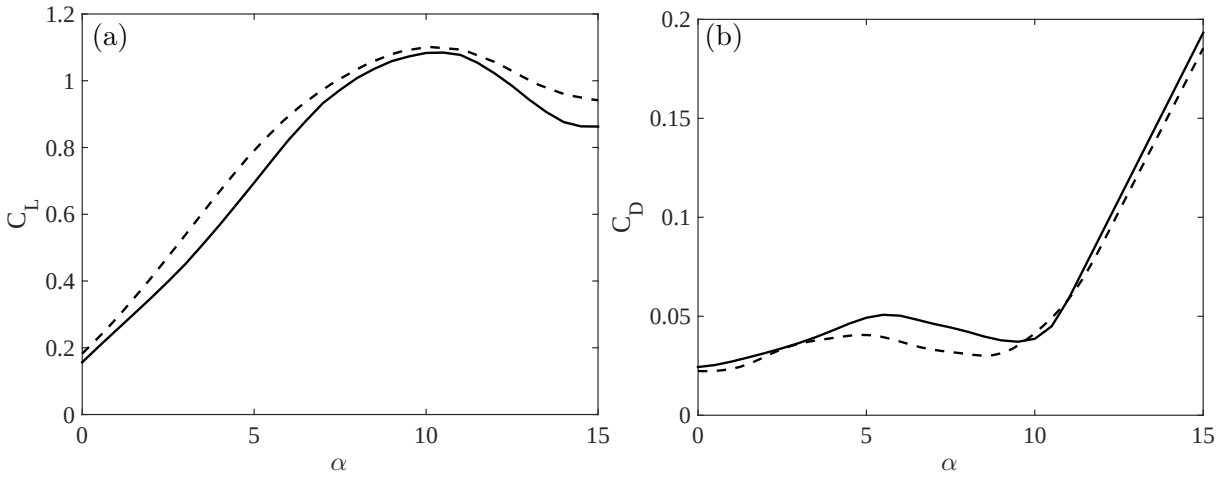

Figure 4. (a) Lift and (b) drag coefficient distributions of A18 airfoil. Re_c=30,000 (—) and Re_c=40,000 (**- -**). The drag coefficients for $Re_c = 30000$ are obtained using XFOIL computations while the rest of aerodynamic coefficients are measurements reported by Selig *et al.* [8].

of the blade tip vortex, from which the vortex core size parameter $a_{\max}$, i.e., the radius of maximum azimuthal velocity can be found. The comparison shows some differences, but overall the experimental and numerical results are very close.

Figure 8 shows the downstream evolution of the tip vortex circulation, calculated inside a circle of diameter $0.2R_0$ around the vortex centre (circle in figure 7a), and of the core radius $a_{\max}$. The circulation values agree well, even if it was not possible to extract experimental data further downstream. Although, some discrepancies in the trend can be seen the level is in general correct. The core radius is of the same order of magnitude in the near wake. In the simulations, a slight dependence on the grid resolution was found, and the core size increases with downstream distance. Part of this increase can be explained by the viscous diffusion of vorticity. The core growth associated with this effect can be estimated by considering a two-dimensional Lamb-Oseen vortex, with Gaussian vorticity distribution of the form $\omega_\theta(\rho) = (\Gamma/\pi a^2)\exp(-\rho^2/a^2)$. The core radius a, which is linked to the radius $a_{\max}$ of maximum swirl velocity by $a_{\max} \simeq 1.12a$, increases in time according to $a^2 = 4\nu(t - t_0)$, where t_0 is a virtual origin of time. Since the downstream convection velocity of the tip vortices is given by $f_0 h$, time t can be related to the

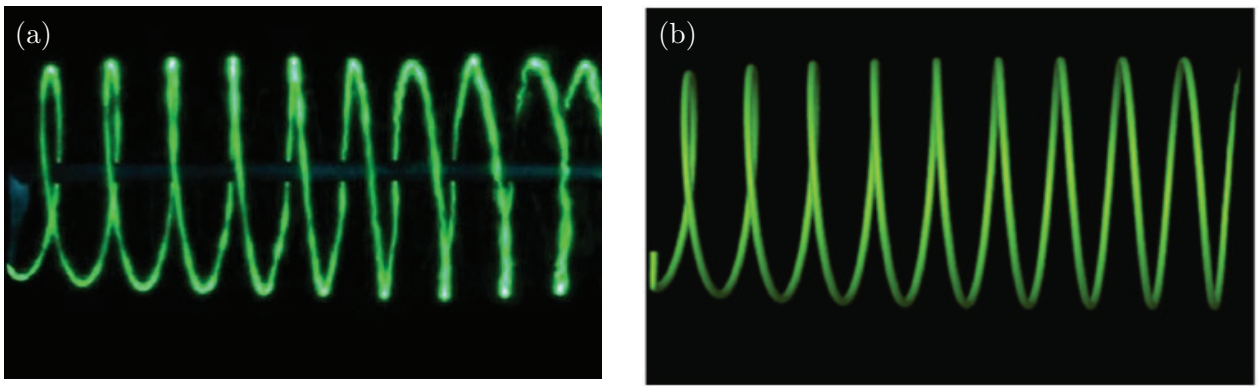

Figure 5. Visualisation of the helical vortices: (a) experiment and (b) numerical computation.

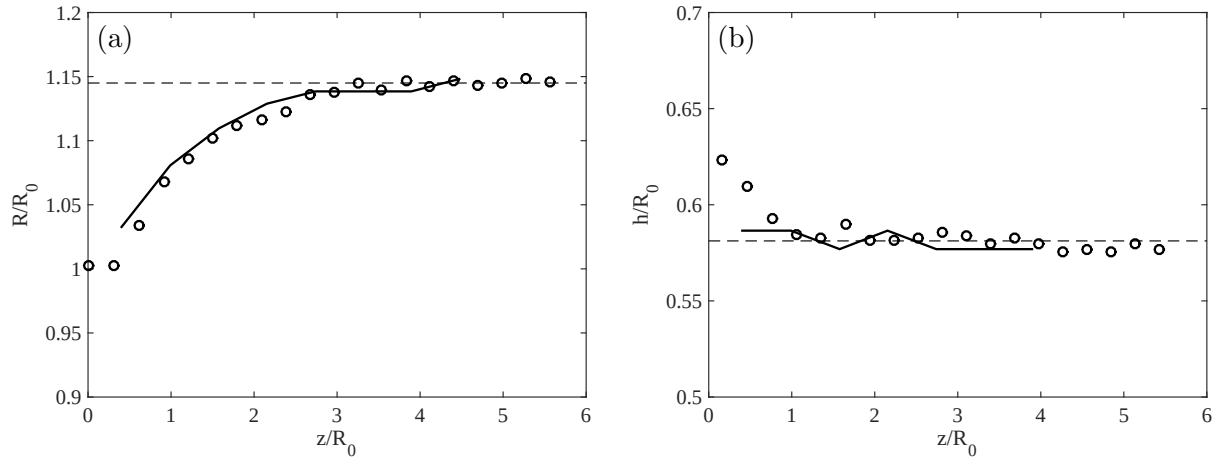

Figure 6. Downstream evolution of helix parameters: (a) radius and (b) pitch. Experiment (○) and numerical computations (—).

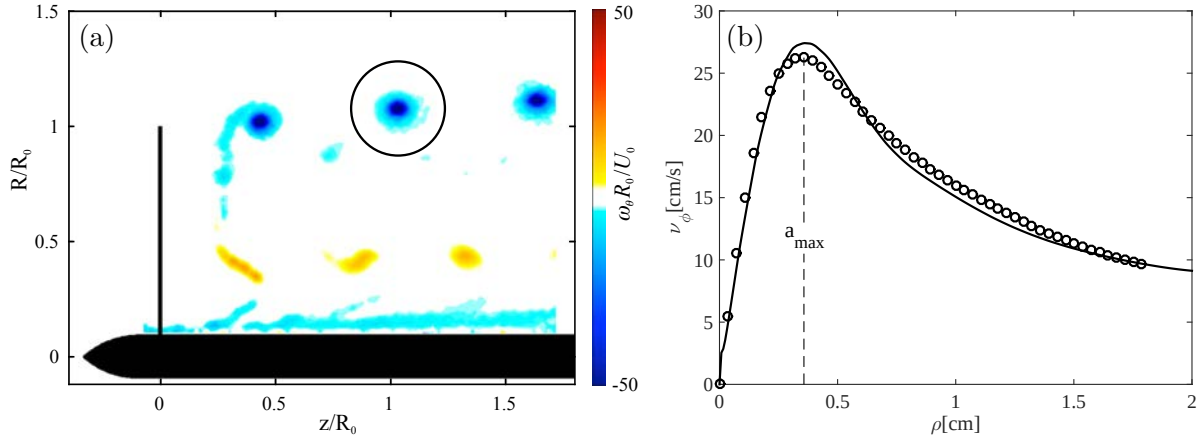

Figure 7. (a) Measured azimuthal (θ) vorticity in the central plane of the rotor. (b) Azimuthal (ϕ) velocity of the vortex inside the circle in (a): experiment (○) and numerical computation (—).

axial position z by $t = z/(f_0 h)$. The dashed line in figure 7(b) represents a fit of the experimental data to the theoretical growth given by $a_{\max} = 1.12\{4\nu[(z/R_0)f_0/(h/R_0) - t_0]\}^{1/2}$, with t_0 as fitting parameter. The faster growth observed in the simulations is possibly linked to an increased diffusion of vorticity due to the numerical scheme.

4.2. Near wake comparison

Figure 9 shows the wake development behind a rotor using the time-averaged azimuthal vorticity.

Figure 10 clearly shows the axial velocity deficit behind the rotor. From figures 9 and 10, it is clear that there is a disagreement in the position of the root vortices. The reason for this will be further discussed in the next section.

Considering the velocity field development, figure 11 shows profiles of axial velocity at three different streamwise positions. The outer wake region shows an increase of velocity due to blockage effects, which is well captured by the numerical computations. The main differences are observed in the region $0 < r/R_0 < 0.5$, which is related to the respective positions of the root vortices.

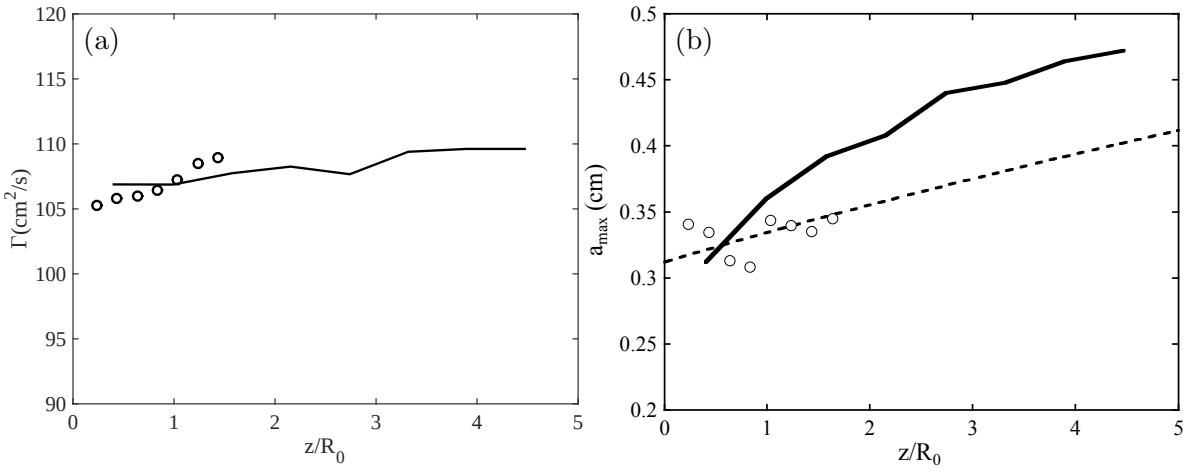

Figure 8. Vortex parameters, (a) circulation and (b) core size as determined from figure 7: experiment (○) and numerical computations (—). The dashed line in (b) represents the theoretical core growth of a Gaussian vortex.

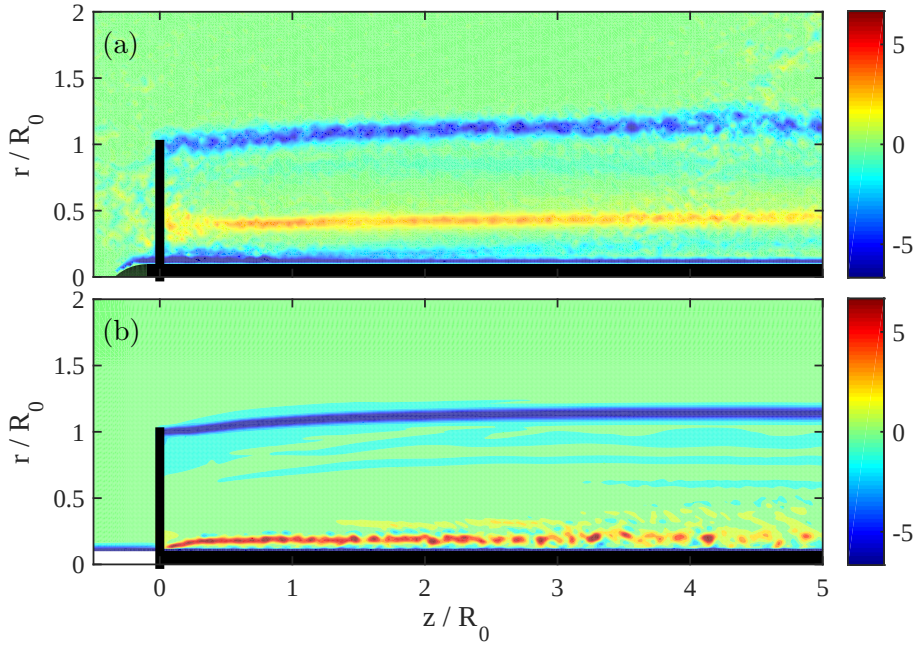

Figure 9. Azimuthal vorticity $\omega_\theta R_0/U_0$: (a) experiment and (b) numerical computation.

Figure 12 shows the axial velocity in the direction along the vortex centre line inside the tip vortices. Figure 12(a) contains the simulation results, extracted from the first four vortex cores in a plane orthogonal to the vortices. The averaged values from these curves are then depicted in figure 12(b), where it is compared to the experimentally observed profile. The profiles show a velocity deficit in the vortex core in the frame of reference of the blade, presumably due to losses in the blade boundary layers, represented by the blade drag. It is observed that the maximum axial velocity is significantly larger, and the profile narrower in the experiments. The total momentum loss (area under the curves) is of the same order in both cases, but it is about 30% higher in the experiments. The shape of the axial velocity profile in the simulations may

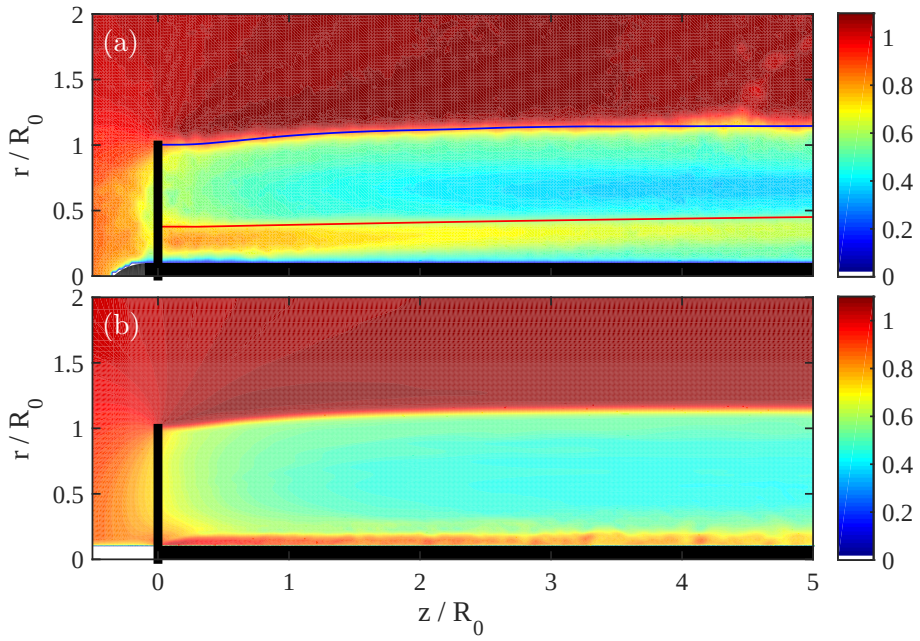

Figure 10. Axial velocity u_z/U_0: (a) experiment and (b) numerical computation.

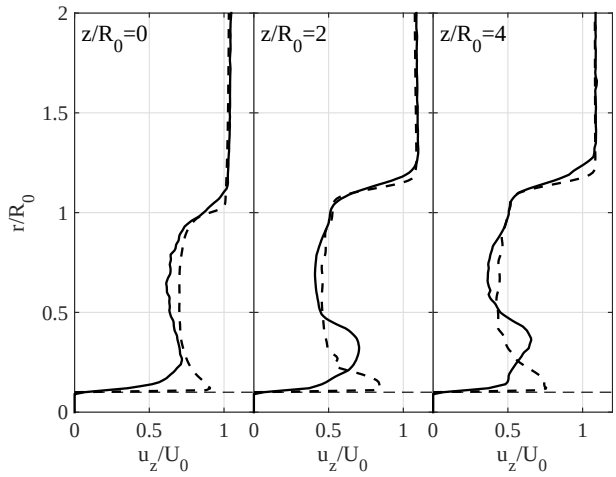

Figure 11. Axial velocity profiles computed at different streamwise positions along the wake. experiment (**- -**) and numerical computations (—).

depend on the resolution, and some qualitative difference may arise from the fact that the boundary layers are actually not represented in the actuator line approach. This aspect needs to be investigated in more detail.

5. Discussion and Conclusions

From the comparisons in the preceding section, it is clear that, when assuming a pitch misalignment of 1.5°, the experimental and simulated results of wake expansion, circulation, helical pitch, tip core properties, as shown in figures 6 to 8, are in very good agreement.

However, when considering the azimuthal vorticity in figure 9 and the axial velocity in figure 10, there is evidence that the root vortex radial position is closer to the rotor axis for the

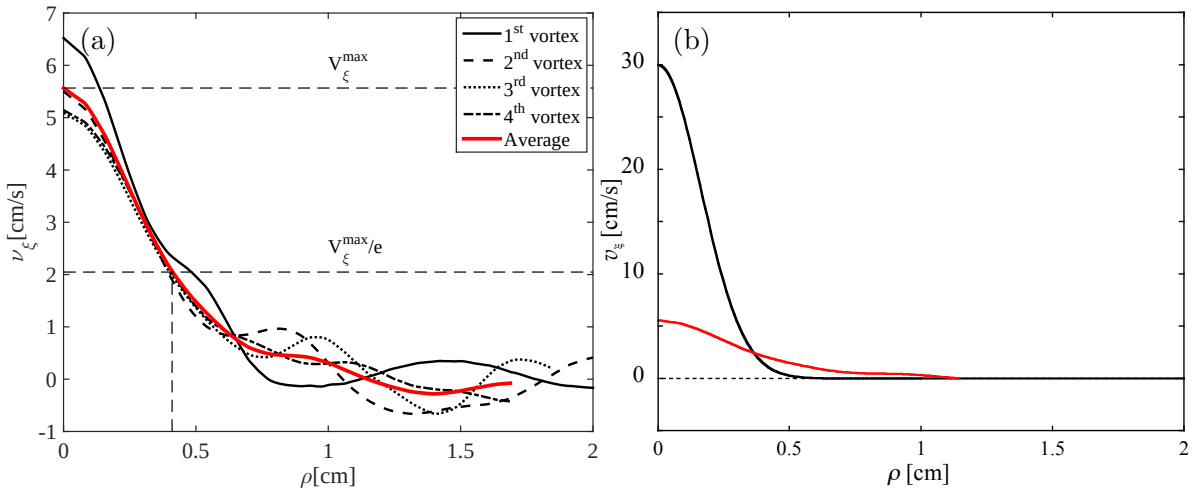

Figure 12. Axial velocity ξ of the vortex: (a) numerical computations profiles of first 4 vortices and (b) experiments (—) and numerical computations (—).

simulations compared to the experiments. This is further illustrated in figure 11, where the flow behaviour is shown at three axial positions. There can be two explanations for this. First, the centre shaft (see figure 1a), used to support the experimental rotor, is rotating at the same angular velocity as the rotor. This has been taken into account in the simulations by applying no-slip conditions in the rotation frame of reference at a radius corresponding to the shaft position in the experimental setup. There are some discrepancies with the actual experimental setup concerning the tip of the shaft extending in front of the rotor (compare figures 9a and 9b). However, the effect of this is found to be small. The simulation setup is based on an LES simulation method, combined with a body force approach. The original reason for this approach is to avoid resolving the boundary layers with the LES method. The mesh has been refined in this area but not to the extent of resolving all scales in the boundary layer. This is therefore considered to be one probable explanation for the different position of the root vortex.

The second explanation could be the body fore approach itself. The actuator line method distributes the body forces along a line representing the blades. The model turbine used in the experiment does, however, have a rather large solidity compared to a modern wind turbine. The blade chord extension is, in the inner part, significantly larger than the number of node points that the loading is applied on. This may result in an unphysical vortex roll-up process, causing a root vortex position that does not correspond to the experimental result.

The present investigation has resulted in good agreement between the experiment and numerical modelling, except for the position of the root vortex and the axial velocity along the centre line of the tip vortex. This study sets a good base for further work on more fundamental stability parameters of the tip vortex. The influence of the root vortex position needs to be further investigated. This study has indicated two possible limitations in the comparison and the numerical modelling. This also results in a good base for further studies of limitations of the actuator line method, as well as of the influence from the boundary layers in LES simulations.

Acknowledgments
This work is supported by the French *Agence Nationale de la Recherche* through the A*MIDEX grant (ANR-11-IDEX-0001-02), project LABEX MEC (ANR-11-LABX-0092) and project HELIX (ANR-12-BS09-0023-01). The simulations were performed on resources provided by the Swedish National Infrastructure for Computing (SNIC) within the project SNIC 2014/8-5.

References

[1] Widnall S E 1972 *J. Fluid Mech.* **4** 641–663

[2] Leishman G, Bhagwat M J and Ananthan S 2004 *J. Am. Helicopter Soc.* **49** 160–175

[3] Ivanell S, Mikkelsen R, Sørensen J N and Henningson D S 2010 *Wind Energy* **13** 705–715

[4] Sarmast S, Dadfar R, Mikkelsen R, Schlatter P, Ivanell S, Sørensen J and Henningson D 2014 *J. Fluid Mech.* **755** 705–731

[5] Sørensen J N, Mikkelsen R F, Henningson D S, Ivanell S, Sarmast S and Andersen S J 2015 *Philosophical Transactions of the Royal Society A: Mathematical, Physical and Engineering Sciences* **373** 20140071

[6] Leweke T, Bolnot H, Quaranta U and Dizès S L 2013 (Lyngby, Denmark: Int. Conf. on Aerodynamics of Offshore Wind Energy Systems and Wakes)

[7] Bolnot H 2012 *Instabilités des tourbillons hélicoïdaux: application au sillage des rotors* Ph.D. thesis Aix-Marseille Université Marseille, France

[8] Selig M S, Guglielmo J J, Broeren A P and Giguere P 1995 *Summary of Low-Speed Airfoil Data* (SoarTech)

[9] Quaranta H U, Bolnot H and Leweke T 2015 *J. Fluid Mech.* (submitted)

[10] Sørensen J N and Shen W Z 2002 *J. Fluid Eng.* **124** 393–399

[11] Mikkelsen R 2003 *Actuator Disc Methods Applied to Wind Turbines* Ph.D. thesis Dept. of Fluid Mech., Technical University of Denmark, DTU

[12] Michelsen J A 1994 Block structured multigrid solution of 2D and 3D elliptic PDE's Tech. Rep. AFM 94-06 Dept. of Fluid Mech., Technical University of Denmark, DTU

[13] Sørensen N N 1995 *General purpose flow solver applied to flow over hills* Ph.D. thesis Risø National Laboratory Roskilde

[14] Ta Phuoc L 1994 *Proc. of the DRET conference: 'Aérodynamique Instationnaire Turbulents - Aspects Numériques et Expérimentaux*

[15] Hansen M O L, Sørensen J N, Voutsinas S, Sørensen N and Madsen H A 2006 *Progress in aerospace sciences* **42** 285–330

[16] Sarmast S 2014 *Numerical study on instability and interaction of wind turbine wakes* Ph.D. thesis KTH, Stability, Transition and Control